



AE CHARACTERIZATION OF BENDING FRACTURE PROCESS IN SiC/SiC COMPOSITES WITH TRANSPIRATION COOLING STRUCTURE

Toshimitsu HAYASHI, Shuichi WAKAYAMA
Tokyo Metropolitan University

Keywords: *Acoustic Emission, Polymer Impregnation and Pyrolysis, Chemical Vapor Infiltration, SiC/SiC Composites*

Abstract

The effect of the volume fraction of the matrix on the bending fracture process of the 3D-woven SiC/SiC composites was investigated by the acoustic emission (AE) technique. The SiC matrix was made by chemical vapor infiltration (CVI) and polymer impregnation and pyrolysis (PIP). The volume fraction of the matrix is varied by selecting the number of PIP cycles; two (poor), four (standard) and nine (rich). The composites with two and four times of the PIP process can create open channels through thickness which can be utilized for the transpiration cooling.

The detected AE signals during the bending tests were analyzed and correlated with the observed micro-damages. As a result, the rich matrix composite showed the quickest accumulation of the micro-damage. The poor matrix composite showed the unsteady mechanical behavior accompanied with catastrophic fiber-buckling. The standard matrix composite has excellent characteristics showing the latest initiation of the micro-damages and relative small accumulation of the micro-damages.

1 Introduction

The SiC/SiC composites with the higher heat-resistance have been studied in order to increase the turbine inlet temperature of current jet engines. However, even if the conventional Ni-based parts are replaced with the SiC/SiC composites, active cooling is still needed to preserve structural strength, since the temperature capability of the SiC/SiC composites is lower than the hot gas temperature (e.g. 1600°C at turbine inlet). Though metallic parts cooled for the gas turbine engine has vigorously been studied, only a few studies have addressed the adoption of cooling concept to composites (oxide/oxide and C/SiC)[1-3].

It has been reported by the author that the 3D-woven SiC/SiC composite with both chemical vapor infiltration (CVI) and polymer impregnation and pyrolysis (PIP) matrices could create a transpiration cooling structure by selecting four cycles of PIP process and that it showed no decrease in strength during 200 thermal cycling (temperature range; RT ~ 1230°C)[4]. On the other hand, the rich matrix composites without the transpiration cooling structure showed a decrease in strength by 25% during the same 200 thermal cycling [4].

The reasons for the improvement in durability may be as follows: 1) internal thermal stresses may be relaxed in porous composites; 2) internal damages may be suppressed in the composites with four cycles of PIP process under thermo-mechanical loading. This study focuses on the latter possibility. However, the evaluation by the thermal loading is very difficult, because the application of thermal stress can not be interrupted optionally. Thus, in this study, the mechanical bending stress which is similar to the thermal stress is applied to the SiC/SiC composites with three different PIP cycles. From the experimental results, the reason for the improvement in durability will be discussed.

The accumulation of the internal damage in several SiC/SiC composite systems has been extensively studied using AE technique [5-8] by Morscher and the colleagues. They have focused on the matrix cracking behavior during tensile-loading in 2D-woven SiC/SiC composites and 3D-woven melt-infiltrated SiC/SiC composites and suggested the ability of AE monitoring of the initiation and accumulation of the damages in matrix.

In this study, the effects of the volume fraction of the matrix on the bending fracture behavior in the 3D-woven SiC/SiC composites with the transpiration structure were examined by the AE measurement. Comparing the microscopic damages of both the fibers and the matrices with the AE

measurements, the influence of the PIP matrix on microscopic damage progression under flexural loading was investigated.

2 Materials and Experimental Procedures

2.1 Materials and specimens

The SiC/SiC composites used in this study were made of Tyranno™ ZMI SiC fiber (Ube Co.) and SiC matrices. The composites have the 3D-orthogonal weaving structure as shown in Fig.1 schematically. The 3D-woven architecture consists of three layers of X bundles, four layers of Y bundles and Z bundles. In a cross sectioned view of “AA” in Fig.1, three longitudinal X-fiber bundles are shown. The X-fiber bundles are called, upper, middle and lower hereafter. Tensile side is not flat because of the weaving structure, which will result the notch-like geometry deriving stress concentration. The location of the notch-like geometry indicated by dotted circles is called a “corner”.

First, a carbon interface layer derived from the chemical vapor infiltration (CVI) process was coated on the fibers, then the SiC matrices were derived from methyl-trichlorosilane by the CVI process and from polycarbosilane by the several times of the PIP process. The porosity was controlled by varying the number of PIP cycles. The specimens fabricated with 2, 4 and 9 cycles of PIP are called P2(poor matrix), P4(standard matrix) and P9(rich matrix). It is important that P2 and P4 have transpiration cooling structure.

2.2 Experimental Procedure

Figure 2 shows the schematic diagram of the testing system. Four-point bending tests were conducted with inner span of 10 mm and outer span of 30 mm at room temperature in air. Loading was applied along Z-direction under a constant cross-head speed of 0.5 mm/min so that the tensile stress was applied along X-direction. Loading patterns are, 1) loading to fracture, 2) loading up to about 50 or 100 MPa and unloading.

During the test, the AE signals were monitored simultaneously by two AE sensors (resonance frequency, 410 kHz) which were attached on both ends of the sample. The AE signals were amplified by 40 dB and then were transmitted to the AE analyzer.

After the PIP treatments, the specimens were cut out and coated with a thin layer of CVI-SiC. Detailed volume fractions of the specimens are

tabulated in Table 1. The dimensions of the specimen were 50 mm length x 4 mm (approx.) width x 2 mm (approx.) thickness. The width corresponds to the size of 2 pitches of the textures.

The threshold level was set to the value of 0.01 V at the input terminal of the amplifiers. The supporting and loading pins were covered with PTFE tape so that the mechanical noise from the contact points between the pins and the specimen could be eliminated.

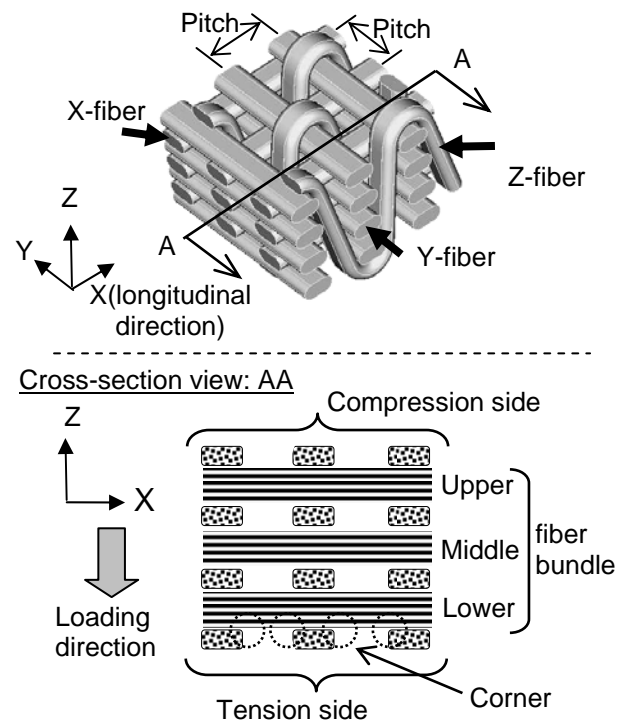


Fig. 1. Schematic diagram of weaving architecture (Fiber volume ratio; X:Y:Z=1:1:0.2, Pitch; 2mm).

Table 1. Volume fraction of fiber, matrix and porosity.

Type	Fiber / %	Matrix / %	Porosity / %
P2	41	29	30
P4	41	34	25
P9	41	46	13

After the bending test, the specimens were soaked in an epoxy resin and kept at 90°C in vacuum for hardening. After the epoxy resin was hardened, the specimens were cut into four pieces with a diamond cutter as shown in Fig.3. The cut surface in the XZ-plane was polished by a 16 μm diamond sheet and then polished by the argon ion-beam(JEOL,SM-09010). The depth of the polished area by the argon ion beam was about 50 μm so that the section mechanically damaged before the ion-beam polishing can be removed.

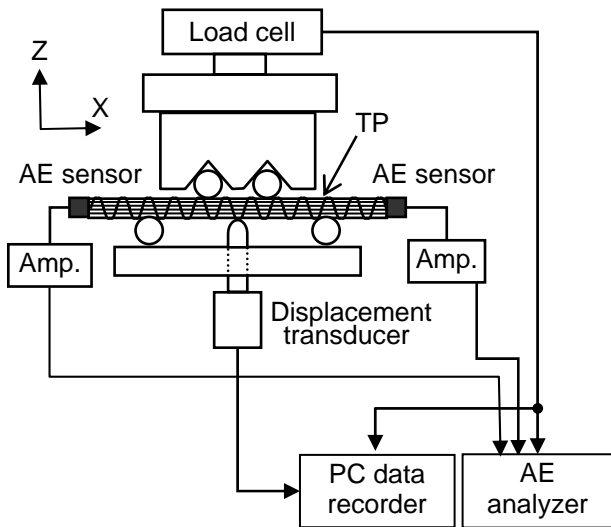


Fig.2. Schematic diagram of bending test apparatus.

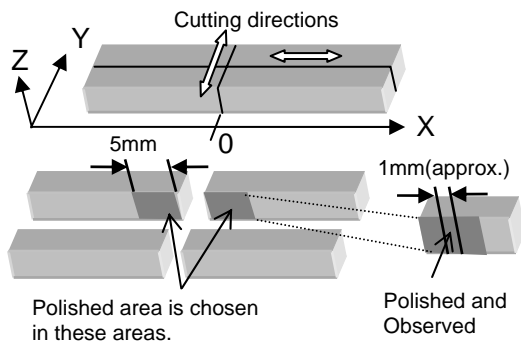


Fig.3. Cutting directions and polished area by the argon ion beam.

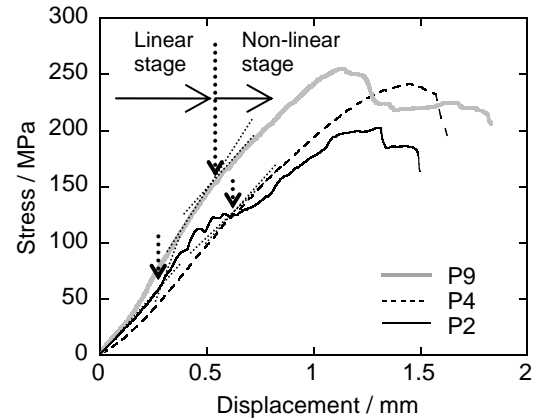


Fig. 4. Stress-displacement curves of the 3D-woven SiC/SiC composites, showing the unsteady behavior in P2.

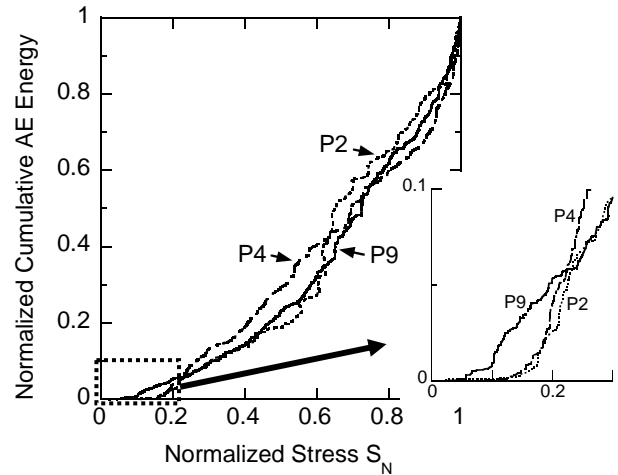


Fig.5. Normalized Cumulative AE Energy vs. Normalized Stress, showing that the AE activity of P9 initiated in the earliest.

3 Results and Discussion

3.1. Mechanical behavior and AE measurement

3.1.1 Loading to fracture

The measured stress-displacement curves for the specimen of P2, P4 and P9, subjected to the bending fracture, are shown in Fig.4. Both a linear section and a subsequent non-linear section were recognized in each stress-displacement curve. The linear section extends to a stress level of about 130MPa and 150MPa for the specimens P4 and P9, respectively and 60MPa for the specimen P2 as indicated by the dotted arrows in the figure. The slope of non-linear sections of P4 and P9 gradually decreased with increasing the displacement. The non-linear part of P2 is fractured, which suggests unsteady deformation behavior.

The normalized cumulative AE energy of P2, P4 and P9 as a function of the stress S_N normalized

by the each fracture stress is presented in Fig. 5. The AE energy accumulated even in the linear stage macroscopically defined by the stress-displacement curves. It suggests that micro-damage is accumulated in the macroscopically linear stress-range. It is worth noting that the accumulation of the AE energy of P9 initiates in the earliest. It indicates that the matrix rich specimen P9 most quickly accumulates the micro-damage in the early stage of loading.

3.1.2 Loading and unloading

Figure 6 shows the measured stress-displacement curves for the specimen, P2, P4 and P9, during loading up to 50MPa(left) and 100MPa(right) and then unloading. The onset of the non-linear

stage was observed only in P2. The onset stress was largely scattered, which suggests the poor matrix composites shows largely unsteady mechanical behavior.

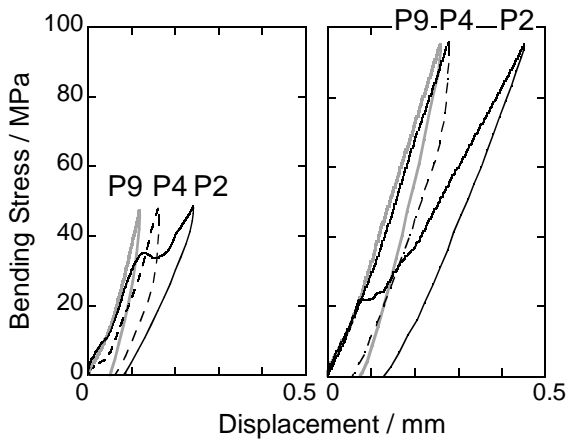


Fig.6. Stress-displacement curves during loading and unloading.

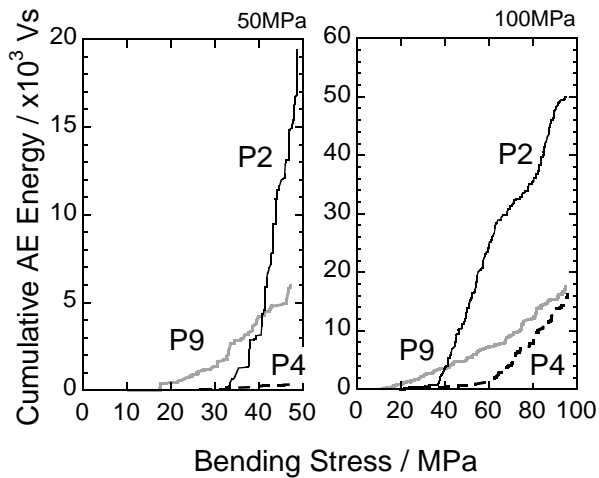


Fig.7. Cumulative AE Energy vs. bending stress during loading to 50MPa(left) and 100MPa (right), showing that the AE activity of P4 was moderate.

Figure 7 shows the AE energy accumulation behavior during loading and unloading. During loading up to 100MPa, the specimen P2 showed a significant AE activity, indicating a large micro-damage accumulation. The standard matrix specimen P4 showed moderate accumulation of the AE energy. It indicates that specimen P4 shows moderate damage accumulation behavior in the early stage of loading.

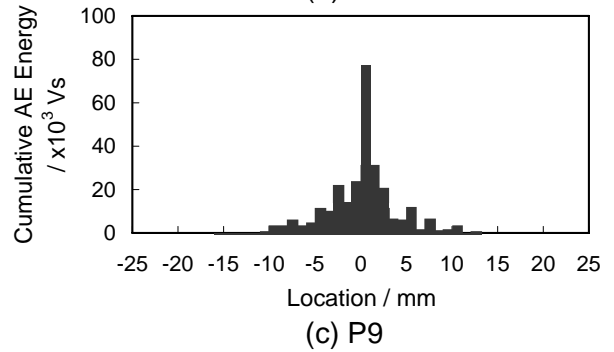
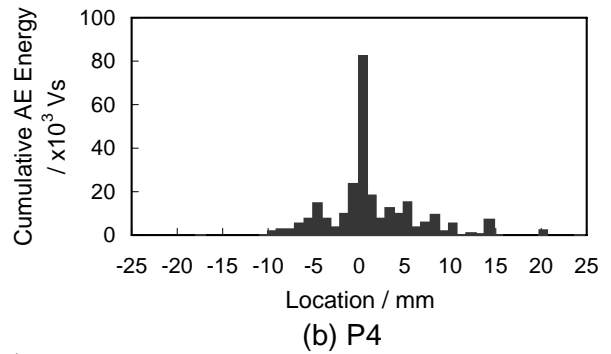
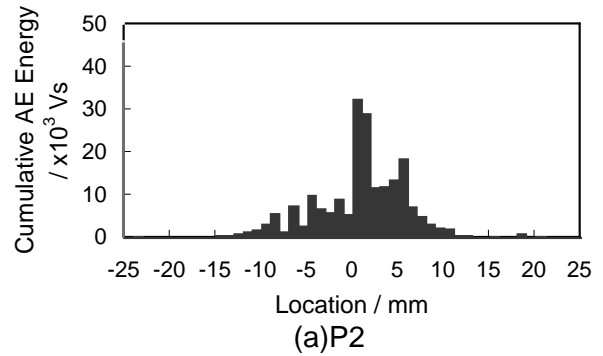


Fig.8. Location of AE events showed by the cumulative AE energy detected during loading up to fracture.

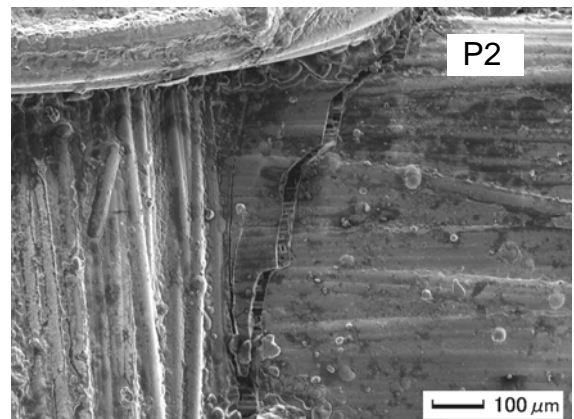


Fig.9. Typical appearance in tension side at the corner which indicates the location defined in Fig.1. The location of the crack shows good agreement with the estimation by the AE measurements.

3.1.3 Location of AE events and macroscopic damages

The histogram of Fig. 8 shows the estimated AE locations in the longitudinal (X) direction versus the accumulated AE energy at the AE location during loading up to fracture in P2, P4 and P9. It is seen that most of the AE events are distributed at the center in the gage section regardless of the PIP cycles.

Figure 9 shows the typical severe macro-damages observed on the tension side. It is seen in the figure that the crack perpendicular to the longitudinal fiber bundle is observed. The severe failure location observed in each specimen nearly coincided to the AE event location at which most of the AE energy was detected.

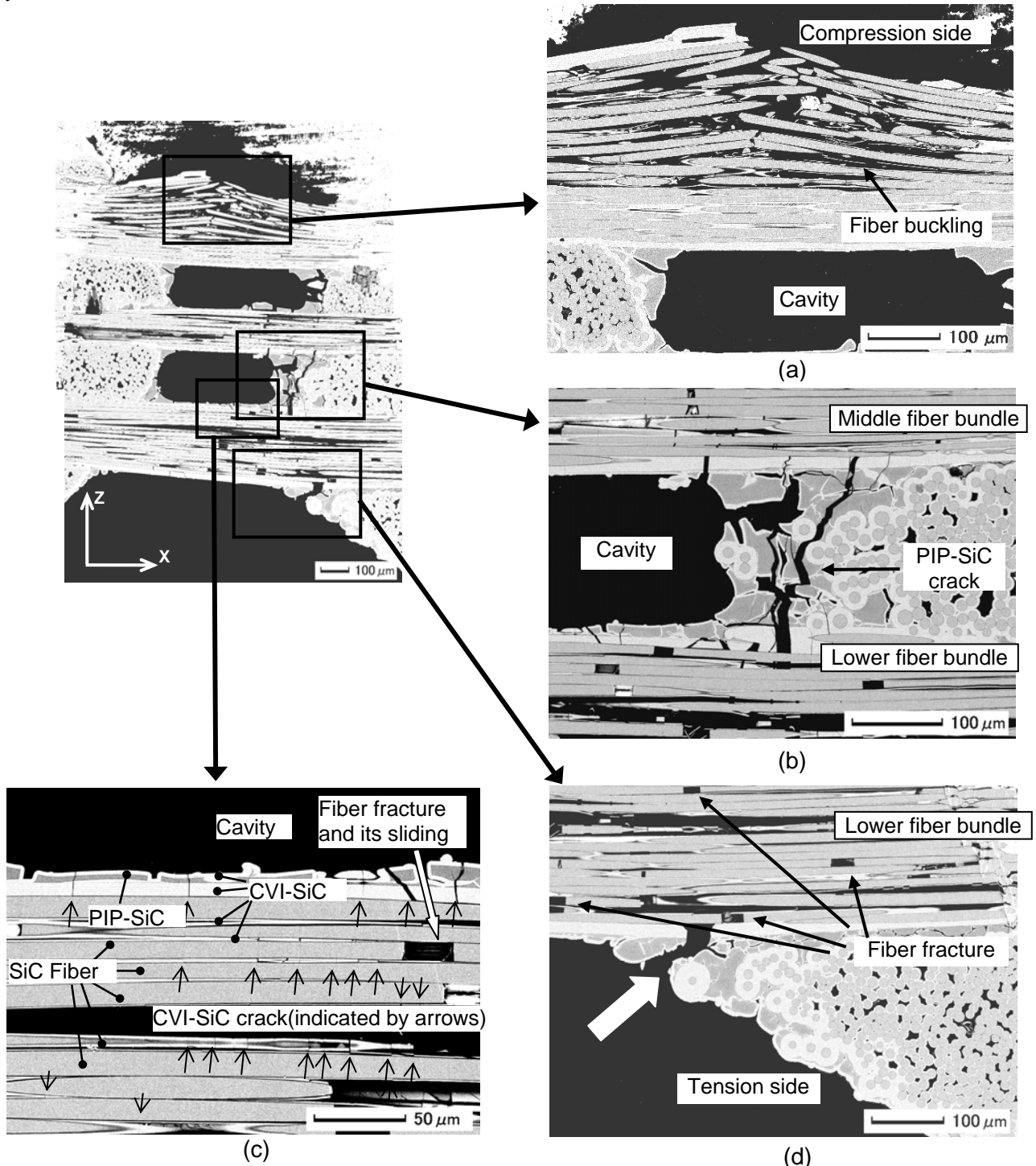


Fig.10. Micrographs of the specimen P2 after the bending fracture.

3.3 Microscopic damages

3.3.1 Microscopic damages in P2

Figure 10 shows the SEM images of the cross section of P2. It is seen that there are a number of cracks widely distributed in the three X-fiber bundles (upper, middle and lower). The fiber-fracture due to buckling (Fig.10(a)) is observed in the upper fiber bundle on the compression side. The crack with the largest opening displacement is found where a white arrow indicates in Fig.10(d) (hereafter this crack is simply called “the corner crack”). The damages in the lower and middle fiber bundles are in the form of the CVI-SiC cracks, the fiber fracture and the fiber sliding in the CVI-SiC matrix as shown in Fig.10(c). In addition, the transverse cracks in the PIP-SiC matrix were observed in Fig. 10(b).

The observed micro-damages in P2 after loading up to 50MPa ($S_N \approx 0.25$) and unloading are shown in the SEM micrographs in Fig.11. The corner cracks were observed.

Figure 12 shows the micro-damages in P2 after loading up to 100MPa ($S_N \approx 0.50$) and unloading. The corner cracks were observed in the figure.

The comparison between the micrographs in Fig.11 and 12 indicates that almost no significant micro-damage was progressed while loading from 50MPa to 100MPa. However, since the AE activity of P2 was observed in a stress range between 50 and 100 MPa as previously shown in Fig.7(right), micro-

damage must have been accumulated in this stress range. Further observation will be carried out to confirm if the micro-damage is progressed in the stress range.

3.3.2 Microscopic damages in P4

Figure 13 shows the micrographs of the polished cross section of P4. The CVI-SiC cracks in the lower fiber bundle are also observed in Fig.13(a) and (b), however it is apparent that the crack density in the CVI-SiC is smaller than that of P2 shown in Fig.10(c). The corner crack is also observed in Fig.13(b), however the crack opening displacement is small. These observations indicated that the accumulation of the micro-damage in P4 was the most moderate among all specimens.

The micro-damage in P4 after loading up to 50MPa ($S_N \approx 0.2$) and unloading has not been found in the polished cross section. This result shows a good agreement with the moderate AE activity as shown in Fig.7 (left).

Figure 14 shows the SEM micrographs of P4 after unloading from 100MPa ($S_N \approx 0.4$). In the Fig.14(a) and (b), the PIP-SiC crack and the spallation were observed on the compression side. In Fig.14(c), the corner cracks were found. (In the figure, the quantity of the PIP-SiC matrix is seemed to be larger than that in P2. Because the polished plane was unexpectedly near the adjacent Z -fiber bundle, thus the PIP-SiC matrix around Z-fiber bundle is appeared on the micrograph.)

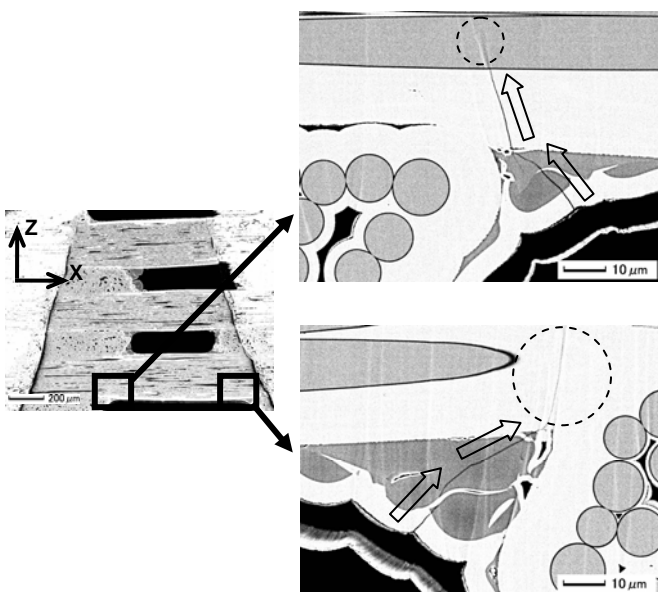


Fig.11. Micrographs of the specimen P2 after unloading from 50MPa showing the corner cracks (Note that the line highlighted by the dotted circle is a trace polished by the argon ion beam).

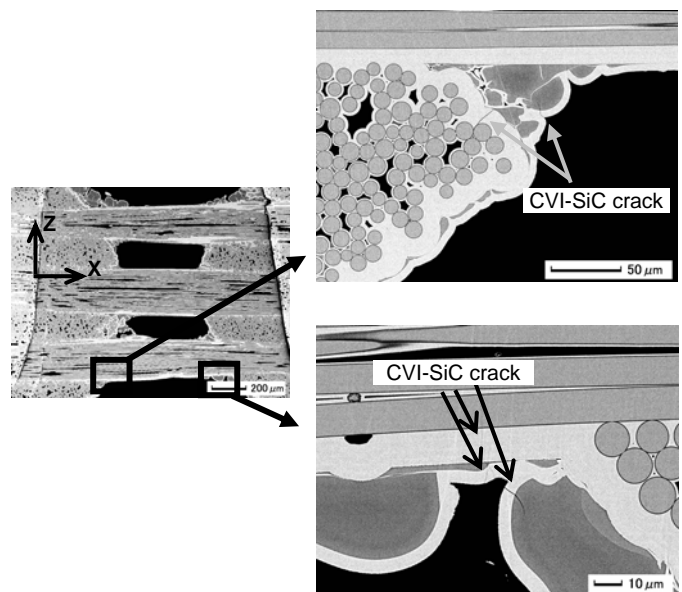


Fig.12. Micrographs of the specimen P2 after unloading from 100MPa showing the corner cracks.

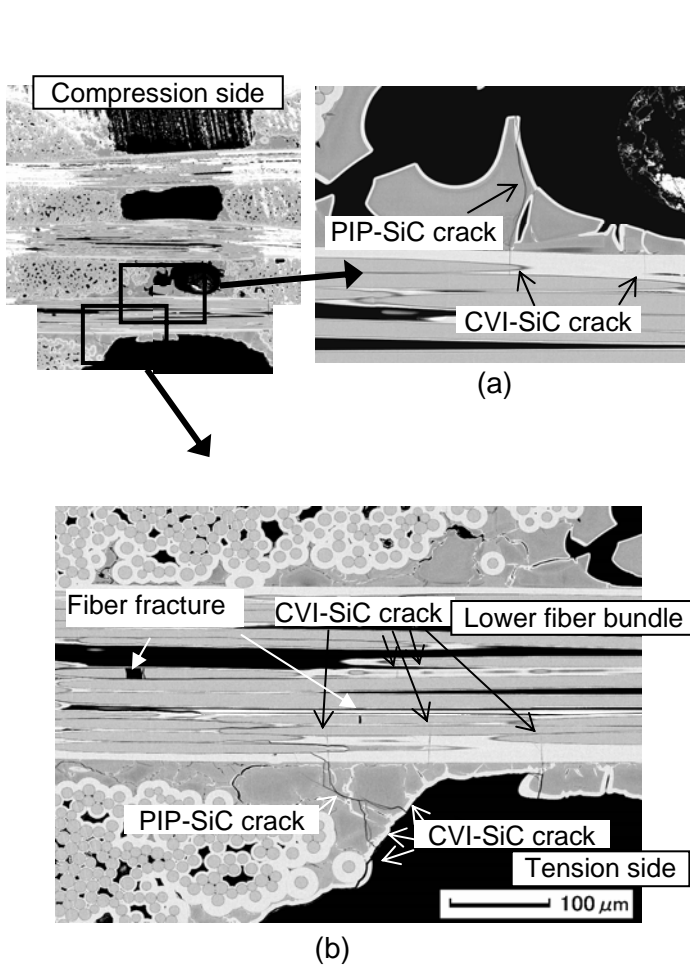


Fig.13. Micrographs of the specimen P4 after the bending fracture showing moderate fracture behavior.

3.3.3 Microscopic damages in P9

The micrographs of the cross section of P9 after the bending fracture are shown in Fig.15. In the Fig.15(a), the spallation of the CVI-SiC coating on the compression side was observed. Figure 15(b) shows a number of cracks in the PIP-SiC matrix. The remarkable PIP-SiC cracks propagate into the middle X-fiber bundle as indicated by the hollow arrows. In the Fig. 15 (c), a number of the CVI-SiC cracks are observed similarly to P2.

The micro-damage after unloading from a stress of 50MPa ($S_N \approx 0.2$) is shown in Fig.16. A crack propagating in the PIP-SiC matrix on the compression side was observed in Fig.16 (a). In the Fig.16(b), the corner crack was observed.

Figure 17 shows the micro-damages observed in P9 after unloading from 100MPa. In the Fig.17(a), the cracks in the PIP- and CVI-SiC matrices were found on the compression side. The corner cracks are observed in Fig.17(b) and (c).

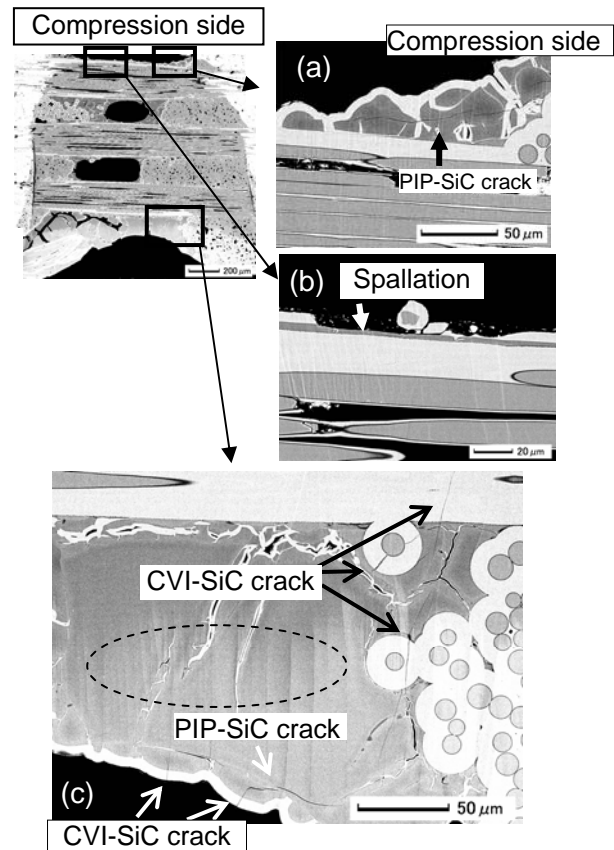


Fig.14. Micrographs of the specimen P4 after unloading from 100MPa (Note that the lines highlighted by the dotted circle are the traces polished by the argon ion beam).

3.3.4 Bending fracture process

The bending fracture behaviors of the SiC/SiC composites having three different volume fraction of the PIP matrix were summarized in the Table 2. The illustrations in the table describe the results of Figs. 10-17, schematically. And the symbols indicate the location of the micro-damage.

It is seen in the table that the corner crack on the tension side is initiated in the early loading stage regardless of the PIP cycles. It indicates that the bending stress in tension side is concentrated to the corner in the early stage of loading.

It is worth noting that the initiation of the micro-damage of P4 was latest and the accumulation of the micro-damage in P4 was relatively small. On the other hand, the matrix rich composites P9 showed the earliest accumulation of the micro-damage.

As mentioned in the introduction, the standard matrix composites P4 which had transpiration cooling structure showed excellent durability under thermal cyclic loading. On the other

hand, the matrix rich composites P9 showed significant decrease in strength during thermal cycling. Although the further investigation on the internal thermal stress is needed, the experimental results in the present study could yield one of the significant reasons for the higher durability of P4.

On the other hand, the micro-damage accumulation in P2 was also as significant as the rich matrix composites P9. Therefore it can not be expected that the poorer matrix composites P2 have excellent durability under thermal cycling.

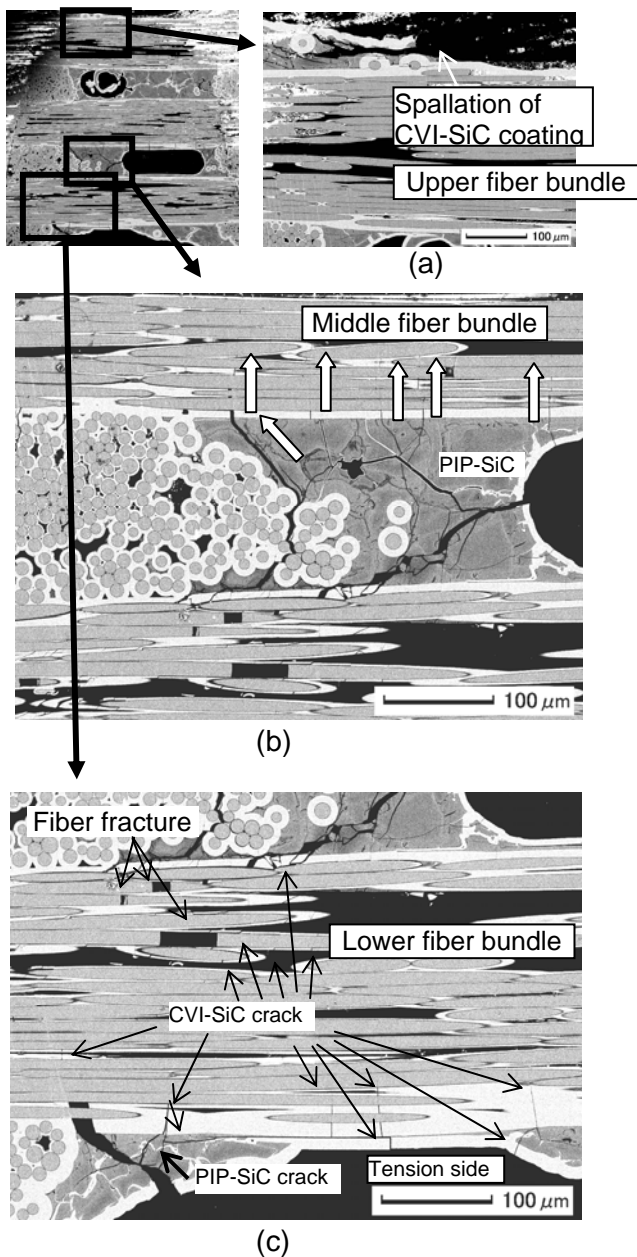


Fig.15. Micrographs of the specimen P9 after the bending fracture.

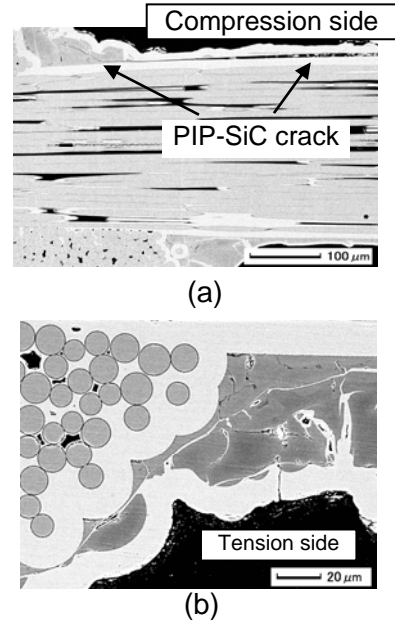


Fig.16. Micrographs of the specimen P9 after unloading from a stress of 50MPa.

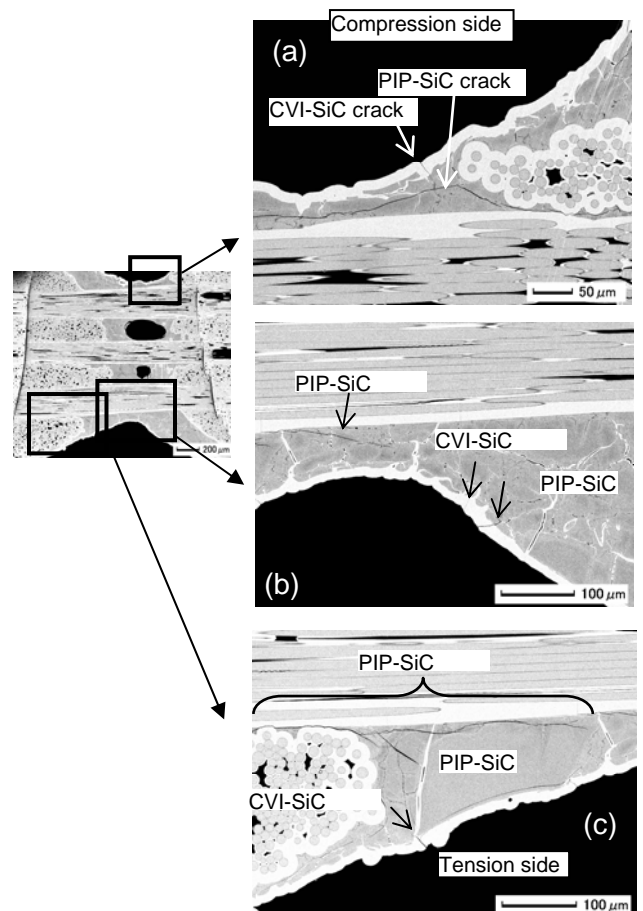
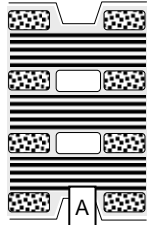
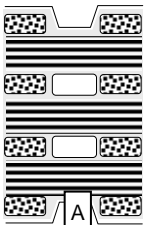
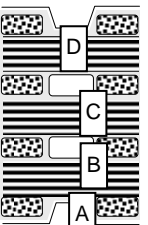
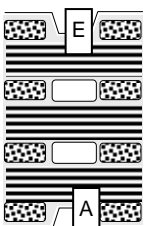
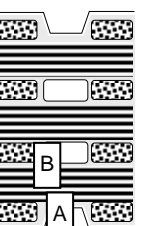
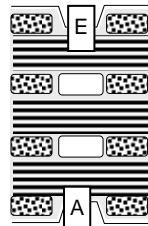
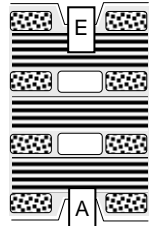
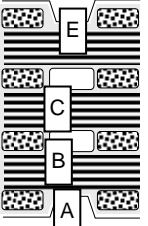


Fig.17. Micrographs of the specimen P9 after unloading from 100MPa

Table 2. Bending fracture process of the SiC/SiC composites with three different PIP repetition cycles.

	50MPa(20N)	100MPa(40N)	Fracture
P2	 <p>A:Corner crack</p>	 <p>A:Corner crack</p>	 <p>A:Corner crack B:CVI-crack, PIP-crack, Fiber Fracture C:CVI-crack D:Fiber buckling</p>
P4	<p>No damage has been found.</p>	 <p>A:Corner crack E:PIP-crack and Spallation</p>	 <p>A:Corner crack B:CVI-crack, PIP-crack and Fiber-fracture</p>
P9	 <p>A:Corner crack E:PIP-crack</p>	 <p>A:Corner crack E:PIP-crack and CVI-crack</p>	 <p>A:Corner crack B:CVI-crack, PIP-crack and Fiber-fracture C:CVI-crack E: PIP-crack , CVI-crack and Spallation</p>

4 Conclusion

The damage accumulation behavior of the SiC/SiC composites with different PIP cycles was examined and following conclusions were obtained.

(1) The standard matrix composites P4 showed the latest micro-damage initiation and moderate

accumulation behavior of the micro-damage. This behavior might result in the higher durability of P4 under thermal cycling.

(2) The poor matrix composites P2 shows unsteady mechanical behavior accompanying a micro-damage of the fiber buckling on the compression side.

(3) The rich matrix composites P9 showed the earliest micro-damage initiation.

(4) The initiation and accumulation of the micro-damage in the SiC/SiC composites could be well detected by AE measurements. The correlation between micro-damage and AE characteristics will be investigated and utilized for the evaluation of fracture mechanism under thermal stress.

References

- [1] Bouchez M., Beyer S., Cahuzac G., "PTAH-SOCAR Fuel-cooled Composite Materials Structure for Dual-Mode Ramjet and Liquid Rocket Engines", *Proc. 40th AIAA/ASME/SAE/ASEE Joint Propulsion Conference and Exhibit*, AIAA 2004-3653, 2004
- [2] Cox B.N., Davis J.B., Marshall D.B., Yand Q.D., "Integral Textile Ceramic Composites for Turbine Engine Combustors", *Proc. ASME TURBO EXPO 2002*, ASME GT-2002-30056, 2002
- [3] Greuel D., Herbertz A., Haidn O.J., Ortelt M., Hald H., "Transpiration Cooling Applied to C/C liners of Cryogenic Liquid Rocket Engines", *Proc. 40th AIAA/ASME/SAE/ASEE Joint Propulsion Conference and Exhibit*, AIAA 2004-3682, 2004
- [4] Hayashi T., "Transpiration cooling structure effects on the strength of 3D-woven SiC/SiC composites under thermal cycling", *Ceram. Eng. Sci. Proc.*, Vol.26, No. 2, pp 335-342, 2005
- [5] Morscher G.N., "Modal acoustic emission of damage accumulation in a woven SiC/SiC composite", *Comp. Sci. Tech.*, Vol.59, pp 687-697, 1999
- [6] Morscher G.N., Yun H.M., DiCarlo J.A., "Matrix cracking in 3D Orthogonal Melt-infiltrated SiC/SiC composites with Various Z-Fiber Types", *J. Am. Ceram. Soc.*, Vol.88, No.1, pp 146-153, 2005
- [7] Morscher G.N., "Stress-dependant matrix cracking in 2D woven SiC-fiber reinforced melt-infiltrated SiC matrix composites", *Comp. Sci. Tech.*, Vol.64, pp 1311-1319, 2004
- [8] Gyekenyesi A.L., Morscher G.N., Cosgriff L.M., "In situ monitoring of damage in SiC/SiC composites using acousto-ultrasonics", *Composites: Part B*, Vol.37, pp 47-53, 2006